論文 / 著書情報
Article / Book Information

Title	Modeling and simulation of polycrystalline ZnO thin-film transistors
Authors	F. M. Hossain,J. Nishii,S. Takagi,A. Ohtomo,T. Fukumura,Hiroshi Fujioka,H. Ohno,H. Koinuma,M. Kawasaki
Citation	Journal of Applied Physics, Vol. 94, No. 12,
発行日/Pub. date	2003, 12
公式ホームページ /Journal home page	http://jap.aip.org/
権利情報/Copyright	Copyright (c) 2003 American Institute of Physics

Modeling and simulation of polycrystalline ZnO thin-film transistors

Faruque M. Hossain,[a),b)] J. Nishii,[c)] S. Takagi,[b)] A. Ohtomo, and T. Fukumura
Institute for Materials Research, Tohoku University, Aoba-ku, Sendai 980-8577, Japan

H. Fujioka
Department of Applied Chemistry, The University of Tokyo, Bunkyo-ku, Tokyo 113-8656, Japan

H. Ohno
Research Institute of Electrical Communication, Tohoku University, Sendai 980-8577, Japan

H. Koinuma
Materials and Structures Laboratory, Tokyo Institute of Technology, Yokohama 226-8503, Japan

M. Kawasaki
Institute for Materials Research, Tohoku University, Aoba-ku, Sendai 980-8577, Japan

(Received 4 June 2003; accepted 1 October 2003)

Thin-film transistors (TFTs) made of transparent channel semiconductors such as ZnO are of great technological importance because their insensitivity to visible light makes device structures simple. In fact, there have been several demonstrations of ZnO TFTs achieving reasonably good field effect mobilities of 1–10 $cm^2/V\,s$, but the overall performance of ZnO TFTs has not been satisfactory, probably due to the presence of dense grain boundaries. We modeled grain boundaries in ZnO TFTs and performed simulation of a ZnO TFT by using a two-dimensional device simulator in order to determine the grain boundary effects on device performance. Polycrystalline ZnO TFT modeling was started by considering a single grain boundary in the middle of the TFT channel, formulated with a Gaussian defect distribution localized in the grain boundary. A double Schottky barrier was formed in the grain boundary, and its barrier height was analyzed as a function of defect density and gate bias. The simulation was extended to TFTs with many grain boundaries to quantitatively analyze the potential profiles that developed along the channel. One of the main differences between a polycrystalline ZnO TFT and a polycrystalline Si TFT is that the much smaller nanoscaled grains in a polycrystalline ZnO TFT induces a strong overlap of the double Schottky barriers with a higher activation energy in the crystallite and a lower barrier potential in the grain boundary at subthreshold or off-state region of its transfer characteristics. Through the simulation, we were able to estimate the density of total trap states localized in the grain boundaries for polycrystalline ZnO TFT by determining the apparent mobility and grain size in the device. [DOI: 10.1063/1.1628834]

I. INTRODUCTION

ZnO has become an attractive wide band gap semiconductor since the demonstration of ultraviolet laser action at room temperature.[1–3] Due to its transparency, ZnO would be of great importance as an active channel layer for the realization of a transparent thin-film transistors (TFTs). Substituting TFTs made of amorphous Si (a-Si) or polycrystalline Si (poly-Si) that are currently used in active-matrix liquid-crystal displays (AMLCDs) with transparent ZnO TFTs would enable improvement in the opening of pixels, resulting in a reduction in power consumption and avoidance of complicated device processing. There have been several experimental studies on ZnO TFTs,[4–8] and the authors have previously demonstrated a reasonably high field effect mobility (μ_{FE}) of 7 $cm^2/V\,s$ in a ZnO TFT (Ref. 8) that has device structure, dimensions, process temperature, and materials set compatible with those of an a-Si TFT. In terms of μ_{FE}, which is higher than that of an a-Si TFT ($\sim$1 $cm^2/V\,s$), the performance of a ZnO TFT is sufficiently good for practical application. However, further study is needed to elucidate the material chemistry and device physics in order to overcome drawbacks such as wide subthreshold characteristics and imperfect channel saturation.

Transparent and conducting polycrystalline ZnO thin films with a (0001) oriented texture can be deposited on glass or flexible plastic substrates using pulse laser deposition at a lower substrate temperature (150 °C)[8] than that (300 °C) used for deposition of a-Si in commercial AMLCDs. These films are composed of nanocrystals with grain size ranging from 50 to 100 nm and consequently have dense grain boundaries (GBs). This dense GB formation has the advantage of developing a semi-insulating film due to overlapping depletion regions, which we will demonstrate in this article. GBs in ZnO generally contain a wide distribution of deep-level traps,[9,10] which are considered to be the main constraints for such improper characteristic performances of

a)Electronic mail: fhossain@imr.tohoku.ac.jp
b)On leave from: Department of Innovative and Engineered Materials, Tokyo Institute of Technology, Yokohama 226-8502, Japan.
c)Also at: Research Institute of Electrical Communication, Tohoku University, Sendai 980-8577, Japan.

ZnO TFTs. We have found that device simulation is the fundamental tool for analyzing the activities of trap states in GBs and their effects on TFT performance. Consequently, we will be able to understand the key factors to improve the performance of ZnO-based TFTs. To the best of our knowledge, there is no report on the effect of GBs and their defect distribution along the band gap on the performance of ZnO-based TFTs. Herein, we report the results of two-dimensional (2D) device simulation of a ZnO TFT using an Atlas device simulator.[11]

There have been many experimental and theoretical studies on poly-Si TFTs and some works on GB modeling and simulation.[12–19] Three basic properties (i.e., a wide band gap, small grain size, and possible existence of deep-level trap states in GBs), make these low temperature-deposited ZnO films qualitatively different from conventional poly-Si thin films. The main differences between ZnO-based TFT modeling and the poly-Si TFT modeling are (i) in a nanocrystalline ZnO thin film, the developed depletion regions around closely spaced GBs overlap to make potential profiles in the film that are different from those of a microcrystalline poly-Si thin film and (ii) due to the wide band gap of ZnO and possible existence of deep-level traps in GBs, the GB potential barrier height modulation with gate bias for ZnO TFTs is different from that of poly-Si TFTs. In the process of development of poly-Si TFTs, many efforts have been made to prevent the formation of GBs in the channel, since GBs of even low density result in large variations in device performance depending on the number and location of GBs in the channel. The GBs are so uniformly distributed in a ZnO-based TFT that it may be possible to overcome the problem even with the presence of GBs, if the characteristics of GBs can be controlled through an understanding of their physical properties and by appropriate chemical modification of them.

In our model, the defects in the crystallite and ZnO-gate insulator interface are assumed to segregate to the GBs; i.e., all of the defects are localized in GBs. This assumption makes our model for GBs in a ZnO thin film equivalent to GBs in a ZnO varistor. Spectroscopic analyses of ZnO varistors[9,10,20,21] and ZnO bulk crystals[22] have revealed that trap levels are located as deep states with ambiguous discrete energy levels. Therefore, it is reasonable to assume here that there is a wide distribution of defect states in the GB with a peak density at the midgap. Here, our discussion will focus on the developed potential profile in the active channel layer of a ZnO TFT and the effects of potential profile on its properties, which will reflect the real microscopic view of ZnO thin film while the TFT is in operational mode. Using our model, we are also able to estimate the unknown trap state densities in GBs by comparing the calculated field effect mobility μ_{FE} and grain size l_g with the experimentally obtained values of them.

II. SIMULATION METHODOLOGY AND MATERIAL PARAMETERS

In the device simulator,[11] the semiconductor parameters are defaulted for silicon. We need to specify the required parameters of ZnO, an active channel layer material, in a TFT structure for a ZnO-based TFT simulation. An experimentally optimized dimensions[8] (channel length $L=5\ \mu$m, channel width $W=25\ \mu$m, active channel layer thickness $t_{\mathrm{ZnO}}=100$ nm, and gate insulator thickness $t_{\mathrm{SiN}}=350$ nm) of a TFT structure is used for 2D device simulation as schematically shown in Fig. 1 to achieve the best TFT performance as required for practical application. Except for the ZnO channel, all material sets and dimensions are identical to those in the *a*-Si TFT, which is used in commercial AM-LCDs. All necessary material constants of ZnO have been collected from different sources[23–29] except for two constants (E_1 and E_2) related to the Gaussian distribution of the defects in the GB as enumerated in Table I. The values of E_1 and E_2 are assumed material constants, to be used throughout this modeling. All energy levels defined in Table I, can be graphically represented by an energy level diagram including a GB energy band bending profile as illustrated in Fig. 2, and are referenced to the valence band edge $E_v=0$. Hence, the GB energy barrier can be defined as, $qV_b=E_{cgb}-E_c=E_{vgb}-E_v$ and the conduction activation energy away from the GB (in flatband region) is represented as, $qV_n=E_c-E_f$ as clarified in Fig. 2, where E_{cgb}, E_c, and E_{vgb} are maximum conduction band energy in the GB, minimum conduction band edge energy in crystallite, and maximum valence band energy in the GB, respectively. The gate insulator Si_3N_4 is a default material in the simulator with given permittivity $\epsilon_I=7.55$.

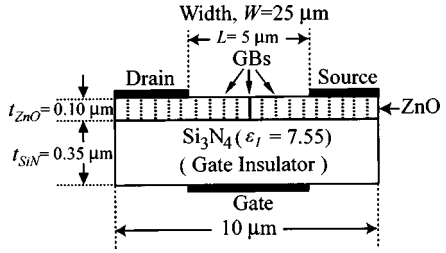

FIG. 1. Schematic cross-section structure of a ZnO TFT for 2D device simulation.

Other material parameters for a polycrystalline ZnO as specified in Table II [i.e., donor density $N_d\,(\mathrm{cm}^{-3})$, grain size $l_g(\mu\mathrm{m})$, and total areal trap state density in GB $N_t\,(\mathrm{cm}^{-2})$], are considered as variables to analyze the device characteristics. The variation of N_d is analogous to the generation of carriers by doping, which is subsequently equivalent to the accumulation or depletion of carriers through the application of gate voltage in the ZnO-based *n*-channel TFTs. The variation of l_g and N_t correspond to the deposition condition of ZnO films and its imperfections, respectively.

The polycrystalline ZnO thin film is defined by introducing equally spaced GBs parallel to the ZnO film thickness and perpendicular to the direction of carrier propagation from source to drain (see Fig. 1). The GB is modeled as a thin layer (i.e., a few atomic layers) having defect states with Gaussian distribution as[11,30]

$$N_{ga}(E)=N_{ta}\exp\{-[(E_{1a}-E)/E_{2a}]^2\}, \tag{1}$$

$$N_{gd}(E)=N_{td}\exp\{-[(E-E_{1d})/E_{2d}]^2\}, \tag{2}$$

$$N_g(E)=N_{ga}(E)+N_{gd}(E), \tag{3}$$

TABLE I. Collected and assumed material parameters (constants) of ZnO for 2D device simulation.

Material constants for ZnO	Value (unit)	Author
Band gap, $E_g(300\,\mathrm{K})$ (E_c-E_v)	3.4 (eV)	Ohtomo *et al.*[a]
Effective mass of an electron in the conduction band, m_e^*	$0.318m_0$	Rode *et al.*[b]
Effective mass of a hole in the valence band, m_h^*	$0.5m_0$	Medelung *et al.*[c]
Dielectric constant, ϵ_s	8.12	Rode *et al.*[b]
Hall mobility, μ_H	150 ($\mathrm{cm^2/V\,s}$)	Hagemark *et al.* and Ohtomo *et al.*[d,e]
Electron affinity, $\zeta(E_{\mathrm{vac}}-E_c)$	4.29 (eV)	Sundaram *et al.*[f]
Work function, $\phi_s(E_{\mathrm{vac}}-E_f)$	4.45 (eV)	Sundaram *et al.*[f]
Donor level, E_c-E_d	30 (meV)	Look *et al.*[g]
Energy level of peak trap state density in GB $E_1[(E_{cgb}-E_{vgb})/2]$	1.7 (eV)[h]	⋯
Characteristic decay energy of Gaussian distribution, E_2	0.25 (eV)[h]	⋯

[a]See Ref. 23.
[b]See Ref. 24.
[c]See Ref. 25.
[d]See Refs. 26 and 27.
[e]References 26 and 27 reported the Hall mobilities for single crystal ZnO are 100 and 200 $\mathrm{cm^2/V\,s}$, respectively, and we use an average value of 150 $\mathrm{cm^2/V\,s}$ in our modeling.
[f]See Ref. 28.
[g]See Ref. 29.
[h]Assumed material constants for ZnO related to the Gaussian defect distribution in the GB.

where subscripts *g*, *a*, and *d* stand for Gaussian distribution, acceptor-like states, and donor-like states, respectively. $N_g(E)$ and E are the density of the defect states and its corresponding trap energy inside the band gap, respectively. N_t, E_1, and E_2 stand for the total density of the trap states, its peak energy, and its characteristic decay energy, respectively. Furthermore, the region between two GBs (crystallite) and ZnO–Si_3N_4 interface is assumed to be completely defect-free. This means, we assume all the defect states are localized in the GBs. For a minimum mesh[31] size of 10 nm (Ref. 12), an areal interface trap density, for example, $10^{11}\,\mathrm{cm^{-2}}$ along the GB, is equivalent to the volume density of $10^{17}\,\mathrm{cm^{-3}}$ in the GB region. We assume an idealized situation that the distribution of both acceptor-like and donor-like defects are the same within the energy gap, i.e., $N_{ta}=N_{td}=N_t$, $E_{1a}=E_{1d}=E_1$, and $E_{2a}=E_{2d}=E_2$. In the simulator, it is assigned that a donor-like trap is positively charged and therefore can only *capture* an electron (i.e., donor-like traps are positive when unoccupied of an electron, but are neutral when occupied). On the other hand, an acceptor-like trap is negatively charged and therefore can only *emit* an electron (i.e., acceptor-like traps are negative when occupied, but are neutral when unoccupied). The *capture* and *emission* processes are handled by the simulator using Shockley–Read–Hall recombination model.[11] The trapping model described earlier is elaborately analyzed by Simmons and Taylor[32] and reported in Werner *et al.*[33] for an *n*-type semiconductor. Therefore, the negative and positive charges in the GB created by trap states are determined by the following probability equations:

$$n_a=\int_{E_v}^{E_c} N_{ga}(E)f(E)dE, \tag{4}$$

$$n_d=\int_{E_v}^{E_c} N_{gd}(E)[1-f(E)]dE, \tag{5}$$

$$f(E)=\frac{1}{1+\exp[(E-E_f)/kT]}, \tag{6}$$

where $f(E)$ is the occupation probability of defect states, E_f is the equilibrium Fermi level, k is the Boltzmann's constant, T is the lattice temperature, and n_a and n_d are the occupied acceptor-like trap state density and unoccupied donor-like trap state density in the GB, respectively. The value of T, considered in this model, is 300 K, i.e., all calculations are performed at room temperature. Hence, the Poisson's equa-

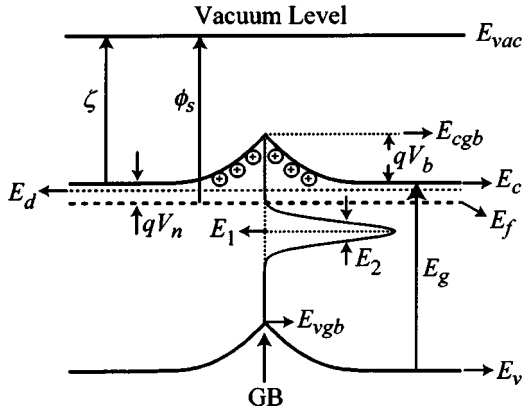

FIG. 2. Energy band diagram for all defined energy levels corresponding to Table I in the presence of a grain boundary. All energy levels are referenced to the minimum energy level $E_v=0$ and the maximum energy level E_{vac}.

TABLE II. Used material parameters (variables) of ZnO for 2D device simulation.

Material variables for ZnO	Symbols (units)	Values
Donor density	$N_d\,(\mathrm{cm^{-3}})$	5.0×10^{14}–1.0×10^{17}
Grain size	$l_g\,(\mu\mathrm{m})$	0.2–1.0
Total areal trap state density in GB (both donor-like and acceptor-like)	$N_t\,(\mathrm{cm^{-2}})$	5.0×10^{11}–1.0×10^{13}

tion to determine the potential profiles along the ZnO channel in the defect-free crystallite regions and in the GB regions are

$$\frac{\partial^2 V}{\partial x^2} = -\frac{q(n-p-N_d^+)}{\epsilon_s} \tag{7}$$

and

$$\frac{\partial^2 V}{\partial x^2} = \frac{q(n-p-N_d^+)}{\epsilon_s} + \frac{qn_t}{\epsilon_s}, \tag{8}$$

respectively, where n, p, N_d^+, and $n_t = n_a - n_d$ are the electron density, the hole density, the ionized shallow donor density, and the net negative charge in the GB, respectively. This net negative charge n_t depletes neighboring electrons of GB and causes exposure of the ionized shallow donors N_d^+, which in turn results in a band bending around the GB. Consequently, a double Schottky barrier is formed at electrostatic and thermal equilibrium. This double Schottky barrier is the main obstacle for the carriers to transport through the polycrystalline ZnO channel. Two different transport mechanisms are utilized for the GB and for the defect-free crystallite regions without any approximation in the device simulator: the thermionic emission process and drift-diffusion process are used for carrier transport over the GB potential barrier and for defect-free crystallite, respectively.

All the physical events described earlier for TFT actions can be numerically analyzed by the device simulator using the following required equations:

$$n = N_c \exp[-(E_c - E_f)/kT], \tag{9}$$

$$p = N_v \exp[-(E_f - E_v)/kT], \tag{10}$$

$$N_d^+ = N_d(1/\{1+\exp[(E_f - E_d)/kT]\}), \tag{11}$$

$$\mathbf{J} = qn\mu\mathbf{E} + qD\nabla n, \tag{12}$$

$$\mathbf{J}_{\mathrm{gb}} = AT^2 \frac{n}{N_c} \exp\left(-\frac{qV_b}{kT}\right), \tag{13}$$

where N_c and N_v are the effective density of states (DOS) for electrons in the conduction band and the effective DOS for holes in the valence band, N_d and E_d are the shallow donor density and its corresponding energy level, $\mathbf{J}$ and $\mathbf{J}_{\mathrm{gb}}$ are the electron current densities in the crystallite and in the GB. μ, $\mathbf{E}$, ∇n, D, and A are the electron mobility, the effective electric field, the electron concentration gradient, the diffusion coefficient for electron, and the electron Richardson constant, respectively. Equations (9) and (10) are the carrier density equations for electrons and holes, respectively. Equation (11) is the occupation probability equation for shallow donors. Equations (12) and (13) are the carrier current density equations describing the drift-diffusion process in the crystallite and the thermionic emission process in the GB, respectively.

Subsequent equations to describe the device characteristics will be based on the earlier basic equations, which can also be efficiently handled by the device simulator without any approximations.

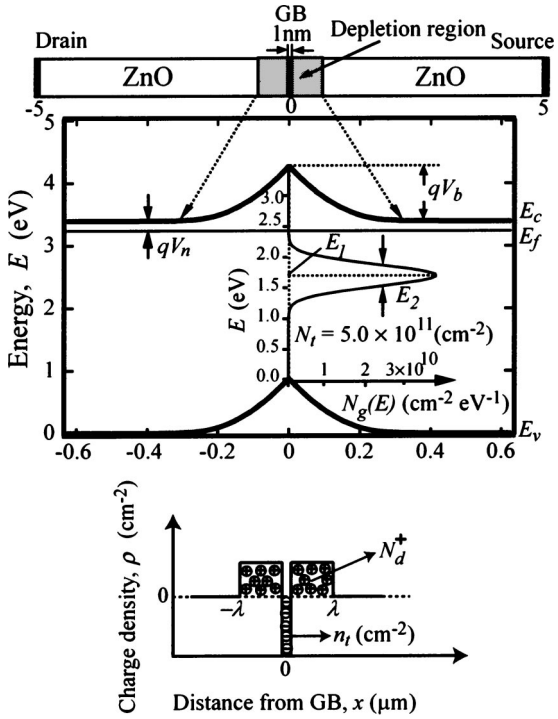

FIG. 3. Energy band bending model of a SGB with Gaussian defect distribution inside the band gap of ZnO, assuming total areal trap state density localized at the GB $N_t = 5.0 \times 10^{11}\,\mathrm{cm}^{-2}$, its peak trap density energy level $E_1 = 1.7$ eV, and its characteristic decay energy $E_2 = 0.25$ eV.

III. RESULTS AND DISCUSSION

A. Single grain boundary modeling

A single grain boundary (SGB) structure of ZnO, setup with materials constants taken from Table I, is modeled in Fig. 3 and can be treated as an *n*-type bicrystal. A 1-nm-thick layer is considered as a GB introducing a Gaussian defect distribution using Eqs. (1)–(3). To simplify the model, we assume $E_1 = 1.7$ eV, $E_2 = 0.25$ eV, using the same distribution for both acceptor-like and donor-like defects. Developed distributed potential $V(x)$ and corresponding electron concentration $n(x)$ are described as a function of distance (x) from the GB to space charge regions as

$$V(x) = V_b \exp\left(-\frac{|x|}{\lambda}\right), \tag{14}$$

$$n(x) = n \exp\left[-\frac{qV(x)}{KT}\right], \tag{15}$$

where λ is the characteristic decay length of distributed potential for gradual depletion and n is the free carrier concentration at thermal equilibrium in the crystallite regions. The values of λ ranges $L_d < \lambda < W_d$, where L_d is the Debye length and W_d is the depletion width, which are usually expressed by the equations

$$L_d = (\epsilon_s kT/q^2 n)^{1/2} \quad \text{and} \quad W_d = (\epsilon_s V_b/qn)^{1/2}, \tag{16}$$

respectively, where ϵ_s is the permittivity of ZnO. The net areal negative charge $n_t\,(\mathrm{cm}^{-2})$ at the GB can be estimated using abrupt depletion approximation and charge neutrality condition, $n_t = 2\lambda N_d^+$ (Ref. 34). For a single GB case, grain

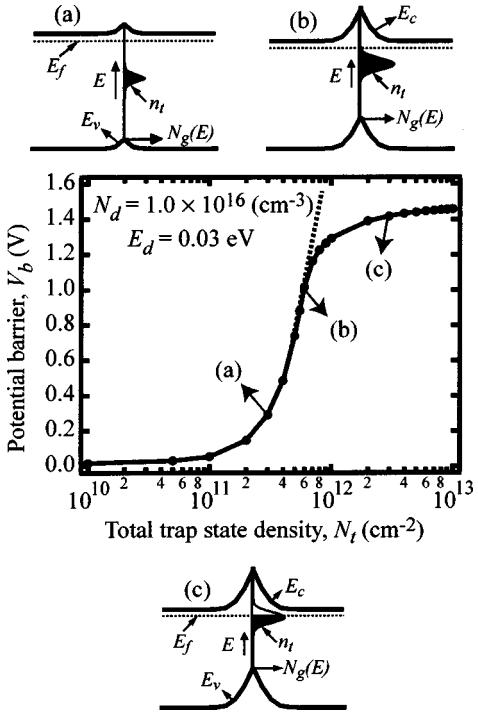

FIG. 4. Change in potential barrier height V_b of a SGB with the total areal trap state density N_t for a fixed donor density $N_d = 1.0 \times 10^{16}\,\mathrm{cm}^{-3}$ and donor level $E_d = 0.03$ eV. The schematics of the three band bending profiles (a), (b), and (c) are drawn corresponding to three different points of the $V_b - N_t$ plot. The dotted line is given by Eq. (17), where all the traps are occupied as shown in (a).

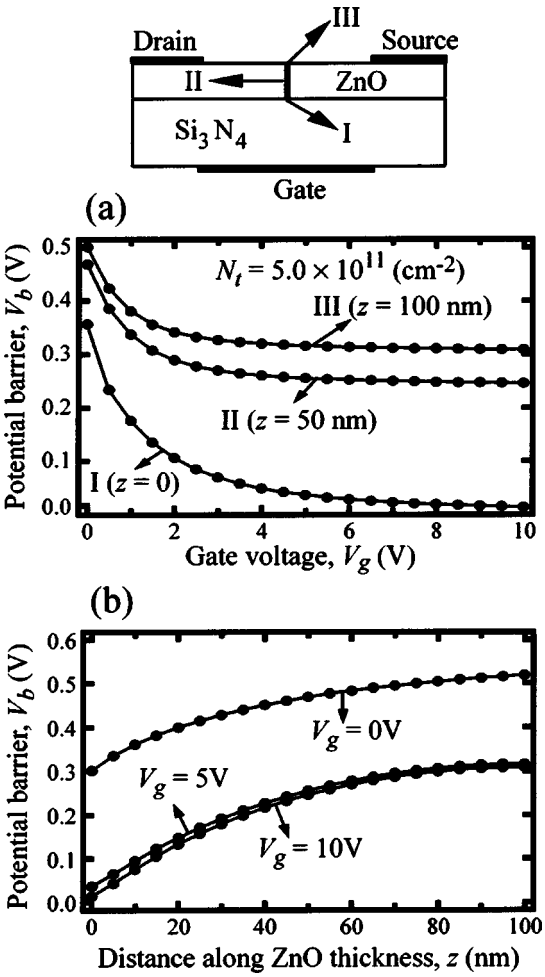

FIG. 5. Change in the potential barrier V_b in a SGB (a) with gate voltage V_g at three locations along the ZnO thickness (I: at the ZnO–Si_3N_4 interface, II: at the middle of the ZnO film, and III: at the surface of the ZnO film) (b) along the ZnO thickness for three different gate bias conditions ($V_g = 0$, 5, and 10 V).

size l_g is large compared to the abrupt depletion length λ, and all the trap states are occupied ($n_t = N_t$), because the Fermi level is above the all trap levels (Fig. 3). In this case, the electrons are depleted partially and the developed potential barrier V_b follows a square relationship with $N_t\,(\mathrm{cm}^{-2})$ as

$$V_b = qN_t^2/8\epsilon_s n = qn_t^2/8\epsilon_s n. \tag{17}$$

The variation of V_b as a function of N_t is a crucial factor to limit the carrier transportation, causing a dramatic change in device performance. Therefore, it is important to explore the maximum limit of V_b with N_t values at the SGB. Figure 4 points up the variation of V_b as a function of N_t for a fixed donor density $N_d = 1.0 \times 10^{16}\,(\mathrm{cm}^{-3})$ and donor level $E_d = 0.03\,(\mathrm{eV})$. Below a certain value of N_t, V_b follows Eq. (17) given by the dotted line because all the trap states are occupied and the established net negative charge at the GB (n_t) remains equal to N_t as illustrated by a schematic band diagram (a). As N_t increases, the calculated curve (solid line) starts to deviate from the dotted line at a critical value of N_t [b]. At much higher N_t values, the trap density levels traverse up the Fermi level resulting in the creation of unoccupied trap states above the Fermi level. The term N_t is then replaced by the term n_t as was described in Eq. (17). Hence, V_b solely depends on the net negative charge n_t in the GB. As the Fermi level impinges deeply into the trap states, as indicated by a schematic band diagram (c), the n_t values start to saturate and correspondingly so does V_b. Charge neutrality conditions are reached after a large trade-off between the affected parameters in Eqs. (4), (5), (6), and (11). Hence, the potential barrier height V_b attains its maximum value under thermal equilibrium conditions. It is worth mentioning that the values of n_a, n_d, and N_d^+ depend on the deposition condition of the ZnO films and the quality of the substrate on which the ZnO films are grown.

To investigate the effect of GBs on TFT properties, it is necessary to calculate how the potential barrier V_b changes in the GB upon applying gate voltage V_g. The top panel of Fig. 5 shows a TFT structure with a SGB located at the middle of the ZnO layer with a Si_3N_4 gate insulator. In this case, we use the values of N_t in GB and N_d for ZnO layer of $5.0 \times 10^{11}\,\mathrm{cm}^{-2}$ and $1.0 \times 10^{16}\,\mathrm{cm}^{-3}$, respectively. Figure 5(a) shows the $V_b - V_g$ curves at three locations in the GB in the ZnO thickness ($z = 0$, 50, and 100 nm). At $V_g = 0$, a change in V_b at three locations is the only effect of band bending due to the work function difference between ZnO and Al gate electrodes.[28,35] As V_g increases, the carriers are accumulated at ZnO–Si_3N_4 interface ($z = 0$), and V_b decreases rapidly, whereas, at the other two locations ($z = 50$ and 100 nm), V_b decreases slowly and becomes independent of V_g. This is due to the fact that the effective field devel-

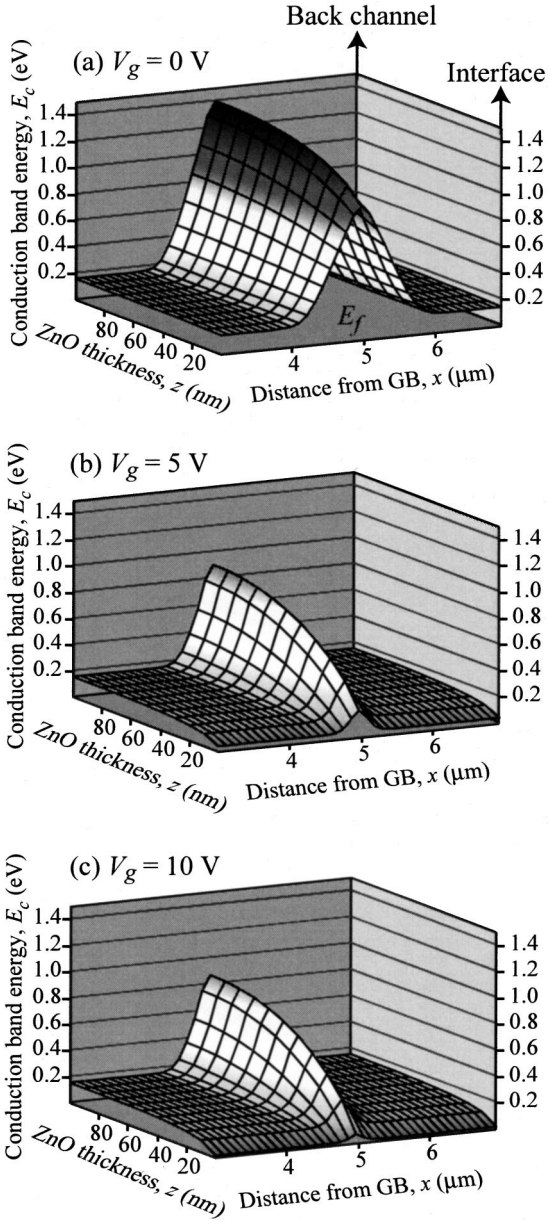

FIG. 6. 3D illustration of the calculated band bending profile in and around the SGB of the ZnO thin film for three different gate bias conditions, (a) gate voltage $V_g = 0$ V, (b) $V_g = 5$ V, and (c) $V_g = 10$ V.

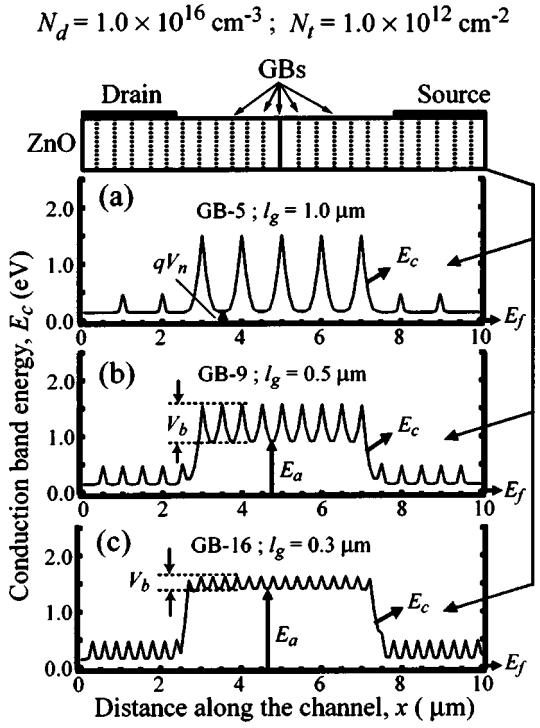

FIG. 7. Potential profile along the surface of the ZnO thin film opposite the source-drain electrodes for three different grain sizes (a) grain size $l_g = 1.0\ \mu$m, with the corresponding effective number of GBs $n_g = 5$ (GB-5), (b) grain size $l_g = 0.5\ \mu$m, $n_g = 9$ (GB-9), and (c) grain size $l_g = 0.3\ \mu$m, $n_g = 16$ (GB-16).

oped by gate bias V_g does not propagate deeply into the channel. Figure 5(b) shows the change in V_b along the thickness of the ZnO film at the GB for three gate voltages ($V_g = 0$, 5, and 10 V). At $V_g = 0$, V_b remains high along the whole thickness, to make a conduction barrier for the carriers. At $V_g = 5$ and 10 V, V_b significantly decreases at the ZnO–Si_3N_4 interface opening up a channel for carrier conduction. These are the fundamental mechanisms of a field effect transistor made using a polycrystalline semiconductor. We also show a three-dimensional (3D) illustration of a calculated band bending profile in Fig. 6 to visualize the combined effect of Figs. 5(a) and 5(b). Three parts of Fig. 6 represent the conduction band profile of the SGB and its neighboring defect-free crystallite regions at the same time as the three gate bias conditions. The Fermi level for the whole region of the ZnO film corresponds to the basal flat plane. The profile along the x direction at the ZnO–Si_3N_4 interface ($z = 0$) illustrates the real view of an actual TFT channel in presence of a single GB, while the profile along the z direction (ZnO thickness) illustrates the bending profile from the ZnO–Si_3N_4 interface to a backchannel of a TFT. The illustrations give graphical interpretation of the measurement of an effective channel width along the active layer thickness. The region at which $V_b + V_n$ is comparable to kT/q can be considered as an effective channel depth from the ZnO–Si_3N_4 interface ($z = 0$). This simple SGB modeling shows a clear insight into trap activity in the GB for a TFT operation and redirects us to model the actual TFT consisting of multiple GBs.

B. Multiple grain boundary modeling

To demonstrate the actual device modeling for the polycrystalline ZnO TFTs, we simulated the effect of multiple GBs. The model of multiple GBs is shown in Fig. 1 where many GBs (dotted lines) are considered along with a SGB (solid line). We find that the behavior of the GB barrier potential and band bending profile for multiple GBs are different from that of the SGB case. All GBs are placed in such a way that they are equally spaced, i.e., the grain size l_g over the entire ZnO film is a constant. Keeping the trap state density in all GBs same as in the SGB, the resulting symmetric barrier potentials at each GB significantly overlap one another, especially, when a condition of $l_g < 2\lambda$ is satisfied. Figure 7 shows a potential profile of a polycrystalline ZnO

thin film for three different grain sizes. For all three cases, the value of N_d and N_t are equal to $1.0\times10^{16}\,\mathrm{cm}^{-3}$ and $1.0\times10^{12}\,\mathrm{cm}^{-2}$, respectively. In Fig. 7(a), the GBs are isolated from each other, i.e., the depletion region associated with each GB are not overlapped. Also, the minimum conduction band energy (activation energy) in the crystallite remains equal to qV_n, which is related to the free carrier concentration n and effective density of states in the conduction band N_c, and represented as

$$V_n=\frac{kT}{q}\ln\frac{N_c}{n}, \tag{18}$$

when the condition $n_t(\mathrm{cm}^{-2})\leqslant N_d(\mathrm{cm}^{-3})l_g(\mathrm{cm})$ is satisfied. In this case, the carrier transport in the film is limited by the thermionic emission over the GB barrier height. It shows the actual view of a microcrystalline thin film, usually observed in a large grain poly-Si thin film. In Fig. 7(b), GBs are more closer than that of Fig. 7(a) and the GB depletion regions are overlapped to lift the minimum conduction band edge E_c up from the equilibrium Fermi level E_f resulting in the activation energy $E_a=E_c-E_f$ higher than the qV_n. Consequently, according to Eq. (9) the concentration of thermally activated carriers become smaller, and then according to Eq. (11) more exposure of ionized donor makes the film semi-insulating due the shifts in Fermi level also away from the donor level E_d. This situation is usually observed in the subthreshold region of transfer characteristics of a TFT. Further reduction of grain size [Fig. 7(c)] establishes a condition $n_t(\mathrm{cm}^{-2})\gg N_d(\mathrm{cm}^{-3})l_g(\mathrm{cm})$, results in lifting up the E_c further away from the E_f, and then the depletion region overlaps to spread over the entire film, leading to very high film resistivity with large thermal activation energy. This situation is usually observed in the off-state region of transfer characteristics of a TFT. If the situation occurs for a particular small-grain thin-film as in Fig. 7(c) without applying any gate bias, then the positive gate bias is required to enhance carriers for operating a TFT. This operational mode of TFT is known as *accumulation mode of operation*. Hence, these three parameters n_t, N_d, and l_g determine the mode (accumulation or depletion) of operation of TFTs. On the other hand, the GB barrier height V_b reduces, because V_b is defined as $E_{cgb}-E_c$ (Fig. 2), which is the energy difference between the conduction band edge minima E_c in the crystallite and the conduction band edge maxima E_{cgb} in the GB. This depicts a realistic potential profile for a nanocrystalline thin film and their properties by reducing l_g or increasing the number of GBs. Hence, one may recognize the distinguishing features between a large-grain microcrystalline poly-Si thin film and small-grain nanocrystalline ZnO thin film for TFT action if these films are used as an active channel layer in the TFT. Therefore, it is important here to note that the grain size, donor concentration, and GB trap state densities are the important parameters for an *n*-type polycrystalline ZnO thin film. These three parameters self-consistently determine the properties of a ZnO thin film, which in turn determine the characteristics of a TFT made using the ZnO thin film. We have already discussed the effect of a GB potential upon changing the trap state density in the SGB case (see Sec. III A). Here we show how the properties of the thin-film change for a fixed number of GBs from source to drain to get a transistor action by changing donor concentration N_d. This is analogous to the carrier modulation on applied gate bias in a TFT structure.

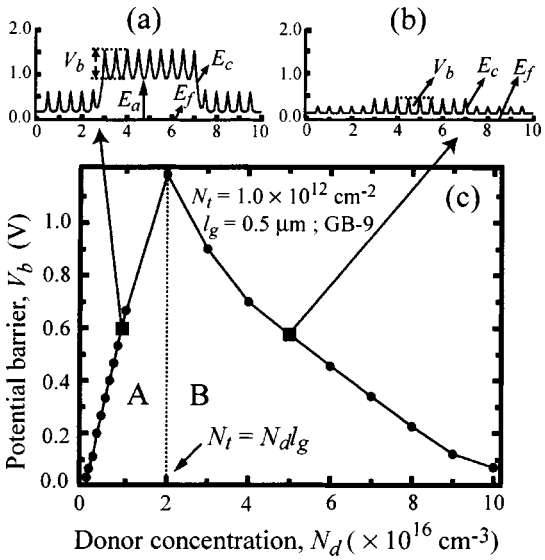

FIG. 8. Plot of the GB barrier height V_b vs the donor density N_d, showing how V_b reaches its maximum value when $N_t=N_d l_g$ for grain size $l_g=0.5\,\mu$m (GB-9) and the GBs potential profiles at two points in regions A and B of V_b-N_d plot.

Figure 8(c) shows the donor concentration N_d dependence on barrier potential V_b for a fixed grain size l_g and a total trap state density N_t at the GBs. The barrier height reaches a maximum at a critical donor density of $N_d=n_t/l_g$. The illustration can be easily divided into two parts (A and B), which are separated by a dotted line. The calculated potential profiles at two representative N_d values [(a) 1.0×10^{16} and (b) $5.0\times10^{16}\,\mathrm{cm}^{-3}$] are represented in Figs. 8(a) and 8(b), respectively. In region A, the depletion regions for each GB are overlapped and a higher activation energy E_a develops, and the GBs become isolated in region B to make the grains partially depleted. The barrier potential for two regions can be represented by[36]

$$V_b=\frac{qN_d l_g^2}{8\epsilon_s}\ (N_d l_g\leqslant n_t)\ \ \text{(proportional to } N_d\text{)}, \tag{19}$$

$$V_b=\frac{qn_t^2}{8\epsilon_s N_d}\ (N_d l_g\geqslant n_t)\ \ \text{(inversely proportional to } N_d\text{)}. \tag{20}$$

Here, we evaluate V_b as a function of N_d, copying the variation of V_b as a function of V_g in TFT structure because both parameters of N_d and V_g are correlated through the shift of Fermi level. Therefore, Figs. 8(a) and 8(b) corresponding to regions A and B represent the potential profiles in the channel of a TFT at subthreshold or off-state and on-state conditions, respectively. The analytical solutions of on-state conductivity or mobility can be obtained for a TFT in presence of GBs using the expression of Eq. (20) with Eqs. (23) and (24) [see Sec. III D] by replacing the donor density N_d with the gate bias assisted accumulation of free carrier density n.

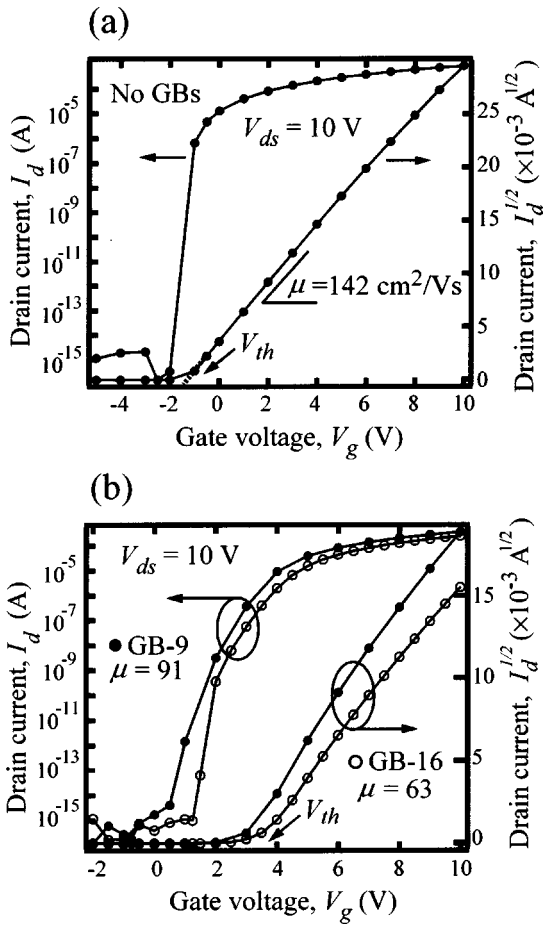

FIG. 9. Transfer characteristics of a modeled ZnO TFT (a) without any GBs (single crystal ZnO TFT) (b) with effective number of GBs (GB-9 and GB-16) within the channel length of the ZnO TFT.

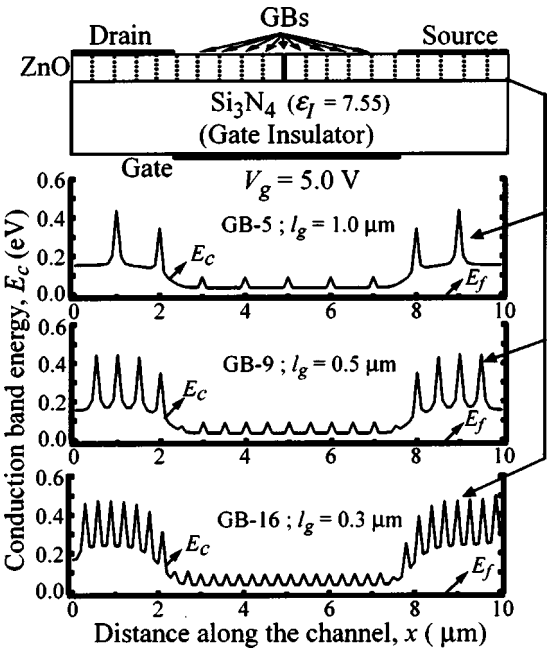

FIG. 10. Potential profile along the ZnO–Si_3N_4 interface, when the gate bias (V_g=5.0 V) is above the threshold for three different grain sizes l_g =1.0, 0.5, and 0.3 μm corresponding to GB-5, GB-9, and GB-16, respectively, within the channel length L.

C. Device characteristics

In light of the earlier modeling and discussions, we have simulated the TFT characteristics taking ZnO as an active material for single crystal (no GB) and polycrystal (with GBs) cases for which schematic device structure is given in Fig. 1. Figure 9(a) shows the transfer characteristics of a single crystal ZnO TFT with a constant drain-source voltage of V_{ds}=10 V. A sharp rise of subthreshold slope and above-threshold linearity of $\sqrt{I_d}$–V_g characteristics indicates the perfect saturation behavior of ZnO channel. The field effect mobility μ_{FE} and the threshold voltage V_{th} are calculated using conventional methods, i.e., from the slope and the x-axis intercept of $\sqrt{I_d}$–V_g curve, respectively. The calculated field effect mobility μ_{FE} is 142 cm^2/V s, which is very close to our considered materials constant (150 cm^2/V s) listed in Table I. This implies that the device simulator can perfectly characterize the TFT properties, and suggests that our model for device characterization is acceptable. Subsequently, the GBs are inserted in the ZnO layer as represented in Fig. 1 to make it polycrystalline and then the transfer characteristics are obtained for 9 and 16 GBs within the channel length of 5 μm as shown in Fig. 9(b). Here, the subthreshold slope shows a considerable tailing, and the $\sqrt{I_d}$–V_g curve deviates from a linear relationship above the threshold voltage; additionally, the threshold voltage shifts to the positive direction of gate voltages. All these effects are more enhanced for more GBs. The μ_{FE} calculated using the maximum slope for GB-9 and GB-16 are 91 and 63 cm^2/V s, respectively. In a similar manner, we can extract the above-threshold mobility for many GBs of nanocrystalline ZnO-based TFTs.

D. Extraction of the GB trap state density

As the most prominent part of this article, we propose an analytical method to extract the GB trap state density from the experimentally obtained TFT characteristics. As we are concerned with the above-threshold mobility, we need to observe the actual potential profiles in a channel when the gate voltage V_g is applied above the threshold voltage V_{th}. Figure 10 elucidates the potential profile at the ZnO–Si_3N_4 interface, where an accumulation channel is formed for three different grain sizes (1.0, 0.5, and 0.3 μm) corresponding to GB-5, GB-9, and GB-16, respectively. In all three cases, mobile carriers from source to drain will only face small potential peaks comparable to kT/q along its direction of propagation. If we apply a low drain-source voltage of V_{ds} =0.1 V, which is far lower than V_g, almost all the GBs remain effective within the channel length L, which we call the linear region. For a relatively high V_{ds} compared with V_g (for instance, V_{ds}=10 V and V_g=5 V), a few GBs near the drain end are diminished due to pinch-off, but the remaining GBs limit the mobility, which we call the saturation region. The simulator can analytically derive the relationship between the mobility and the number of GBs assuming no voltage drop between each GB (in the crystallite). The assumption here is quite reasonable, because the resistance in

the crystallite region above the threshold voltage is much lower than that in the GB region. To establish the relationship, the following equations are used.[37,38]

Current density through the grain boundary barrier is expressed as

$$J_{\mathrm{gb}}=qv_n n\exp(-qV_b/kT)[\exp(q\Delta V_b/kT)-1], \quad (21)$$

where $v_n=AT^2/qN_c$ is the thermal velocity of the electron and ΔV_b is the voltage drop across each GB. Equation (21) replicates Eqs. (12) and (13), and thus it includes both the drift-diffusion and thermionic emission effects of the transport. If the drain bias is high enough to satisfy $q\Delta V_b \gg kT$, Eq. (21) becomes,

$$J_{\mathrm{gb}}=qv_n n\exp(-qV_b/kT)\exp(q\Delta V_b/kT). \quad (22)$$

If there are n_g grain boundaries within the channel length L, then ΔV_b equals V_{ds}/n_g. For a uniform electric field in the channel, the macroscopic (source to drain) conductivity is expressed by

$$\sigma=J_{\mathrm{gb}}L/V_{\mathrm{ds}}=\frac{qv_n nL}{V_{\mathrm{ds}}}\exp(-qV_b/kT)\exp(qV_{\mathrm{ds}}/n_g kT). \quad (23)$$

Equation (23) can be simplified as

$$\sigma=qn\mu^*, \quad (24)$$

where μ^* is a reduced effective mobility, which is limited by the number of GBs n_g in the channel and the GB potential barrier V_b:

$$\mu^*=\frac{v_n L}{V_{\mathrm{ds}}}\exp(qV_{\mathrm{ds}}/n_g kT)\exp(-qV_b/kT). \quad (25)$$

Note that the term $\exp(-qV_b/kT)$, associated with each GB, is gate bias V_g dependent. Above the threshold ($V_g=5$ V), V_b reduces becoming comparable to kT/q for all GBs in the channel (see Fig. 10) and then the contribution of this exponential term to control mobility becomes small for V_g ranges 5–10 V, where we conventionally calculate the field effect mobility μ_{FE}. Another exponential term $\exp(qV_{\mathrm{ds}}/n_g kT)$ remains effective and controls μ^* depending on the number of GBs n_g in the channel, because it integrates all the small contributions of the term $\exp(-qV_b/kT)$ associated with it as mentioned earlier. Thus, μ^* in Eq. (25) represents the field effect mobility, μ_{FE}, at the on-state condition of a TFT. Therefore, it can be stated that the effective number of GBs inside the channel length limits the field effect mobility of the TFTs at its on-state condition. The analytical derivation of Eq. (25) implies that μ_{FE} decreases exponentially as the number of GBs n_g increase.

Finally, we have calculated the field effect mobility from the transfer characteristics of our modeled TFT for the effective number of GBs in the channel considering three different total areal trap state densities N_t in the GBs as illustrated in Fig. 11. Five points are actual simulated data points for three N_t values. Extensions of these data points are exponential extrapolations based on Eq. (25). It is clearly seen that those five points are sufficient for exponential curve fitting. We extend these three curves up to the experimental data range, which are usually extracted from our several ZnO-based TFTs.[8,39] Low temperature-deposited (150–500 °C) nanocrystalline ZnO thin films exhibit GBs ranging in number from 50 to 100 within the channel length $L=5$ μm and the field effect mobilities ranging from 1 to 10 $\mathrm{cm^2/V\,s}$ for a wide range of gate biases. The crossing arrows in Fig. 11 shows the experimental data ranges. If we compare our experimental data with this graph, it is possible to make a rough estimation of the GBs total areal trap state density N_t, which is of the order of $10^{12}\,\mathrm{cm^{-2}}$ for our ZnO-based TFTs. This value is reasonably realistic, about 1% of the total number of surface atoms of a ZnO thin film, which is of the order of $10^{14}\,\mathrm{cm^{-2}}$. Therefore, one can use the graph in Fig. 11 as a rough estimation of GBs total areal trap state densities of any ZnO-based TFTs as soon as one knows their coordinate (mobility as ordinate and effective number of GBs as abscissa) points. A recent report of Carcia *et al.*[7] on rf magnetron sputtered ZnO TFT estimated the total areal trap state densities in GBs ranging from $1.5\times10^{12}\,\mathrm{cm^{-2}}$ to $3.0\times10^{12}\,\mathrm{cm^{-2}}$ and their estimated field effect mobility is 1.2 $\mathrm{cm^2/V\,s}$ for one of their good TFT. This result is also comparable to our simulation result. This re-enforces the consistency between our method of simulation and the experiment for ZnO-based TFT.

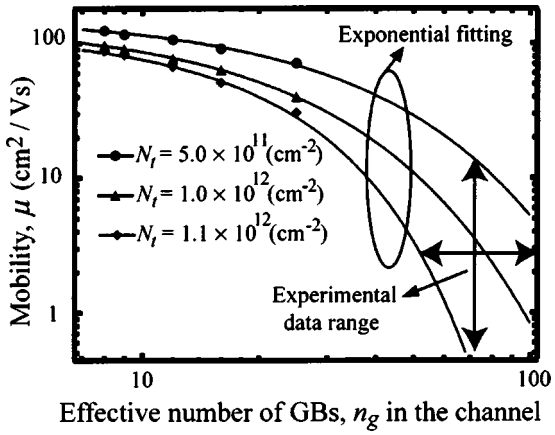

FIG. 11. Calculated mobility μ_{FE} vs effective number of GBs n_g plot for three different total areal trap state density N_t values and the exponential extrapolations [Eq. (25)] up to the experimental data range.

IV. CONCLUSION

Device simulation of ZnO TFTs was performed using the device simulator. An actual polycrystalline ZnO TFT modeling was commenced using a SGB positioned at the middle of the ZnO layer in a TFT structure. A double Schottky barrier formation in the GB adequately described the nature of potential barrier and the spreading of depletion region from the GB to the crystallite for a wide range of trap state densities localized in the GB. The SGB model also suitably described the change of potential profile in and around the GB with applied gate electric field, exhibiting how effectively the channel is formed across the GB. The multiple GB model afterward facilitated the observation of the real microscopic view of a developed potential profile in the nanocrystalline ZnO active layer. We thoroughly explained the action of a nanocrystalline ZnO TFT using our

calculated potential profiles. While our assumption on the trap distribution in the band gap is too simple and crude, it is good enough to visualize the potential profile in the channel upon gate bias application. The most promising option of this simulation is to calculate the approximate range of total areal trap state density localized in GBs by comparing the simulated mobility and grain size with those obtained from experiment on polycrystalline ZnO TFTs, without executing spectroscopic measurement.

The next step would be to analyze the trap distribution through measurement of temperature dependence for the TFT characteristics and compare them with simulation results. That would provide more detailed insight into the trap distribution. Subsequently, one can test some of the chemical modification of the GBs and extract the effects on how the trap distribution is modified.

ACKNOWLEDGMENTS

This work was supported by the MEXT Grant of Creative Scientific Research No. 14GS0204, the Nissan Science Foundation, and Nippon Sheet Glass Foundation for Materials Science and Engineering.

[1] Z. K. Tang, G. K. L. Wong, P. Yu, M. Kawasaki, A. Ohtomo, H. Koinuma, and Y. Segawa, Appl. Phys. Lett. **72**, 3270 (1998).
[2] P. Yu, Z. K. Tang, G. K. L. Wong, M. Kawasaki, A. Ohtomo, H. Koinuma, and Y. Segawa, Solid State Commun. **103**, 459 (1997).
[3] D. M. Bangall, Y. F. Chen, Z. Zhu, T. Yao, S. Koyama, M. Y. Shen, and T. Goto, Appl. Phys. Lett. **70**, 2230 (1997).
[4] Y. Ohya, T. Niwa, T. Ben, and Y. Takahashi, Jpn. J. Appl. Phys., Part 1 **40**, 297 (2001).
[5] S. Masuda, K. Kitamura, Y. Okumura, S. Miyatake, H. Tabata, and T. Kawai, J. Appl. Phys. **93**, 1624 (2003).
[6] R. L. Hoffman, B. J. Norris, and J. F. Wager, Appl. Phys. Lett. **82**, 733 (2003).
[7] P. F. Carcia, R. S. McLean, M. H. Reilly, and G. Nunes, Jr., Appl. Phys. Lett. **82**, 1117 (2003).
[8] J. Nishii, F. M. Hossain, T. Aita, Y. Ohmaki, S. Kishimoto, T. Fukumura, Y. Ohno, H. Ohno, S. Takagi, K. Saikusa, I. Ohkubo, A. Ohtomo, F. Matsukura, H. Koinuma, and M. Kawasaki, Jpn. J. Appl. Phys., Part 2 **42**, L347 (2003).
[9] K. Mukae, A. Ohi, and A. Tanaka, J. Eur. Ceram. Soc. **21**, 1871 (2001).
[10] Y. Wang, W. Lee, and T. Tseng, Appl. Phys. Lett. **69**, 1807 (1996).
[11] Device Simulator, Atlas, Silvaco International, Santa Clara, CA.
[12] K. Yamaguchi, J. Appl. Phys. **89**, 590 (2001).
[13] C. A. Dimitriadis and D. H. Tassis, J. Appl. Phys. **77**, 2177 (1995).
[14] G. A. Armstrong, S. D. Brotherton, and J. R. Ayres, Jpn. J. Appl. Phys., Part 1 **37**, 1721 (1998).
[15] M. Kimura, S. Inoue, and T. Shimoda, J. Appl. Phys. **89**, 596 (2001).
[16] M. Kimura, R. Nozawa, S. Inoue, T. Shimoda, B. O.-K. Lui, S. W.-B. Tam, and P. Migliorato, Jpn. J. Appl. Phys., Part 1 **40**, 112 (2001).
[17] F. V. Farmakis, J. Brini, G. Kamarinos, C. T. Angelis, C. A. Dimitriadis, and M. Miyasaka, IEEE Trans. Electron Devices **48**, 701 (2001).
[18] H.-S. Kong and C. C. Lee, J. Appl. Phys. **78**, 6122 (1995).
[19] T.-J. King, M. G. Hack, and I.-W. Wu, J. Appl. Phys. **75**, 908 (1994).
[20] Y. Ohbuchi, T. Kawahara, Y. Okamoto, and J. Morimoto, Jpn. J. Appl. Phys., Part 1 **40**, 213 (2001).
[21] J. C. Simpson and J. F. Cordaro, J. Appl. Phys. **63**, 1781 (1988).
[22] V. Gavryushin, G. Raciukaitis, D. Juodzbalis, A. Kazlauskas, and V. Kubertavicius, J. Cryst. Growth **138**, 924 (1994).
[23] A. Ohtomo, K. Tamura, K. Saikusa, K. Takahashi, T. Makino, Y. Segawa, H. Koinuma, and M. Kawasaki, Appl. Phys. Lett. **75**, 2635 (1999).
[24] D. L. Rode, Semicond. Semimetals **10**, 1 (1975).
[25] Landolt-Bornstein, in *Semiconductors*, edited by O. Medelung (Springer, Berlin, 1998), Vol. III-17, pp. 35–115.
[26] K. J. Hagemark and L. C. Chacka, J. Solid State Chem. **15**, 261 (1975).
[27] A. Ohtomo, H. Kimura, K. Sato, T. Makino, Y. Segawa, H. Koinuma, and M. Kawasaki, J. Cryst. Growth **214/215**, 284 (2000).
[28] K. B. Sundaram and A. Khan, J. Vac. Sci. Technol. A **15**, 428 (1997).
[29] D. C. Look and J. W. Hemsky, Phys. Rev. Lett. **82**, 2552 (1999).
[30] M. Kimura, S. Inoue, T. Shimoda, and T. Sameshima, Jpn. J. Appl. Phys., Part 1 **40**, 49 (2001).
[31] The mesh is defined by a series of horizontal and vertical lines and the spacing between them in a 2D structure. The crossing points of horizontal and vertical lines are called mesh points.
[32] J. G. Simmons and G. W. Taylor, Phys. Rev. B **4**, 502 (1971).
[33] J. Werner and M. Peisl, Phys. Rev. B **31**, 6881 (1985).
[34] P. Chattopadhyay, J. Phys. Chem. Solids **56**, 189 (1995).
[35] Z. M. Zhao, R. L. Jiang, P. Chen, W. P. Li, D. J. Xi, S. Y. Xie, B. Shen, R. Zhang, and Y. D. Zheng, Appl. Phys. Lett. **77**, 3140 (2000).
[36] H. Ikeda, J. Appl. Phys. **91**, 4637 (2002).
[37] P. V. Evans and S. F. Nelson, J. Appl. Phys. **69**, 3605 (1991).
[38] R. L. Petritz, Phys. Rev. **104**, 1508 (1956).
[39] S. Takagi, J. Nishii, Y. Ohno, H. Koinuma, H. Ohno, and M. Kawasaki, Extended abstracts, JSAP, Spring Meeting, 2002, p. 324.